



**HAL**  
open science

## Structural and physical properties of the high pressure perovskite layered Sr 4 Cr 3 O 10 chromate

Justin Jeanneau, Christophe Lepoittevin, André Sulpice, Stéphanie Kodjikian, Pierre Toulemonde, Manuel Núñez-Regueiro

► **To cite this version:**

Justin Jeanneau, Christophe Lepoittevin, André Sulpice, Stéphanie Kodjikian, Pierre Toulemonde, et al.. Structural and physical properties of the high pressure perovskite layered Sr 4 Cr 3 O 10 chromate. Journal of Solid State Chemistry, 2017, 251, pp.164-169. 10.1016/j.jssc.2017.04.016 . hal-01534594

**HAL Id: hal-01534594**

**<https://hal.science/hal-01534594>**

Submitted on 22 Sep 2021

**HAL** is a multi-disciplinary open access archive for the deposit and dissemination of scientific research documents, whether they are published or not. The documents may come from teaching and research institutions in France or abroad, or from public or private research centers.

L'archive ouverte pluridisciplinaire **HAL**, est destinée au dépôt et à la diffusion de documents scientifiques de niveau recherche, publiés ou non, émanant des établissements d'enseignement et de recherche français ou étrangers, des laboratoires publics ou privés.

# Structural and physical properties of the High Pressure perovskite layered $\text{Sr}_4\text{Cr}_3\text{O}_{10}$ chromate

Justin Jeanneau<sup>a,b,\*</sup>, Christophe Lepoittevin<sup>a,b</sup>, André Sulpice<sup>a,b</sup>, Stéphanie Kodjikian<sup>a,b</sup>,  
Pierre Toulemonde<sup>a,b</sup>, Manuel Núñez-Regueiro<sup>a,b</sup>

<sup>a</sup> Université Grenoble-Alpes, Institut Néel, F-38000 Grenoble, France

<sup>b</sup> CNRS, Institut Néel, F-38000 Grenoble, France

\* Corresponding author.

E-mail address : justin.jeanneau@neel.cnrs.fr

## ABSTRACT

We report on the structure and physical properties of a bidimensional chromate,  $\text{Sr}_4\text{Cr}_3\text{O}_{10}$ , the  $n=3$  member of the Ruddlesden-Popper  $\text{Sr}_{n+1}\text{Cr}_n\text{O}_{3n+1}$  series. For the first time, using complementary x-ray powder diffraction and electron diffraction data, we have solved its layered crystallographic structure. Our study shows also that this high pressure phase is insulating and antiferromagnetic below  $T_N=280\text{K}$ , a similar behavior already observed for  $n=1, 2$  and  $n=+\infty$  members.

## Keywords :

High Pressure – High Temperature Synthesis; Layered materials; Precession Electron Diffraction, Powder X-ray diffraction; Magnetization; Electrical transport.

## 1. Introduction

The layered oxides derived from the perovskite structure constitutes a large family of compounds that yields an extremely rich physics. In such a structure the  $\text{MO}_2$  (with  $M$  = transition metal element) layer always plays an essential role. For the case of 3d elements this family was at the origin of the discovery of high  $T_c$  superconductivity in the cuprates [1] or giant magnetoresistance in manganates [2,3]. Recently we have started a more detailed study of the different members of the Ruddlesden-Popper series based on chromium,  $\text{Sr}_{n+1}\text{Cr}_n\text{O}_{3n+1}$  [4]. Few reports exist in the literature on these chromates because High Pressure – High Temperature (HP-HT) is needed for their synthesis. In  $\text{Sr}_3\text{Cr}_2\text{O}_7$  ( $n=2$ ) we have reported an anomalous asymmetric distortion of the  $\text{CrO}_6$  octahedra associated to simultaneous orderings of the orbital and spin degrees of freedom [5]. We focus here on the isolation of the phase  $\text{Sr}_4\text{Cr}_3\text{O}_{10}$  ( $n=3$ ) and its structural and magnetic characterizations. It was previously only detected as an intergrowth in

high resolution transmission electron microscopy (HRTEM) images of  $\text{Sr}_3\text{Cr}_2\text{O}_7$  [6]. Thanks to a combined X-ray and electron diffraction study, we have resolved the crystallographic structure of this  $n=3$  member. In addition, we show that  $\text{Sr}_4\text{Cr}_3\text{O}_{10}$  (Sr4310) is an insulator with an antiferromagnetic (AFM) transition at  $T_N=280\text{K}$ .

## 2. Experimental

The synthesis of layered chromates is difficult, as it requires HP-HT techniques. Our samples were prepared using a large volume press with toroidal “Conac 28” anvils [7,8]. A stoichiometric mixture (4:3) of SrO (Sigma Aldrich 99%) and  $\text{CrO}_2$  (Sigma Aldrich 99%) was pressed into a pellet and introduced in a gold capsule. Our polycrystalline samples were treated at HP-HT in the 4-6 GPa range and  $1100^\circ\text{C}$  for 30 min. The conditions were optimized to increase the amount of the Sr4310 phase.

Powder X-ray diffraction experiments were performed on a D5000T diffractometer working with the  $\text{Cu K}_\alpha$  wavelength ( $\lambda_\alpha = 1.5406 \text{ \AA}$ ). Data were collected at room temperature, in a  $2\theta$  angular range from  $10.00^\circ$  to  $90.32^\circ$ , with a  $0.032^\circ$  step size.

For TEM analysis, the specimen was prepared by crushing a small piece of sample in an agate mortar containing ethanol, and a drop of the suspension was deposited on a copper grid covered with a holey carbon film. Electron transmission microscopy was performed on a LaB<sub>6</sub> Philips CM300ST Transmission Electron Microscope (TEM) operating at 300kV, equipped with a  $\pm 30^\circ$  double tilt sample holder and the Nanomegas spinningstar precession device (with a precession angle of  $2.5^\circ$  for our experiments). Images and Selected Area Electron Diffraction with and without Precession (SAED and PED) patterns were recorded using a F416 TVIPS camera, and the Energy Dispersive Spectroscopy (EDS) spectra were recorded on a Brüker Silicon Drift Detector. Reflection intensities extraction on PED patterns was performed using ELD module from CRISP software and merging process was carried out with TRIPLE, both software belong to the Calidris package [9]. The final hkl dataset was used as an input in the direct method structure determination software SIR2011 [10] to calculate “ab initio” the structural model.

The magnetic properties of our samples were measured in a Metronique Ingenierie SQUID with a sensitivity of  $10^{-7}$  emu at low field and  $10^{-5}$  emu at high field. Electrical resistivity measurements were performed using the four contacts (with epoxy-silver paint) technique using a DC current of  $10\mu\text{A}$ .

## 3. Results and discussion

We now focus our discussion on the properties of our sample containing the maximal amount of Sr4310, around  $\sim 23\%$  (see results of the final Rietveld refinement below), for the P,T conditions used (i.e. elaborated at 4GPa and  $1100^\circ\text{C}$ ). Its powder XRD pattern and the corresponding Rietveld refinement are shown on Fig. 1. Most of the main diffraction peaks can be indexed with the perovskite structure  $\text{SrCrO}_3$ . Nevertheless, the reliability factors of the

refinement are not good ( $R_{\text{Bragg}} = 5.17\%$  and global  $\chi^2 = 19.2\%$ ). Indeed, the remaining Bragg peaks, evidenced on the the difference curve (between the calculated and observed intensities), do not fit to the precursors nor any other phase present in the crystallographic database. They correspond to the reflections of the Sr4310 phase not overlapped with the ones of the perovskite. By analogy with the isostructural  $\text{Sr}_4\text{Ti}_3\text{O}_{10}$  ( $a = 3.90 \text{ \AA}$  and  $c = 28.1 \text{ \AA}$ ) of the Ti-based series  $\text{Sr}_{n+1}\text{Ti}_n\text{O}_{3n+1}$  [11,12] a first estimation of the tetragonal lattice parameters of Sr4310 can be made:  $a = 3.82(2) \text{ \AA}$  and  $c = 27.8(5) \text{ \AA}$ .

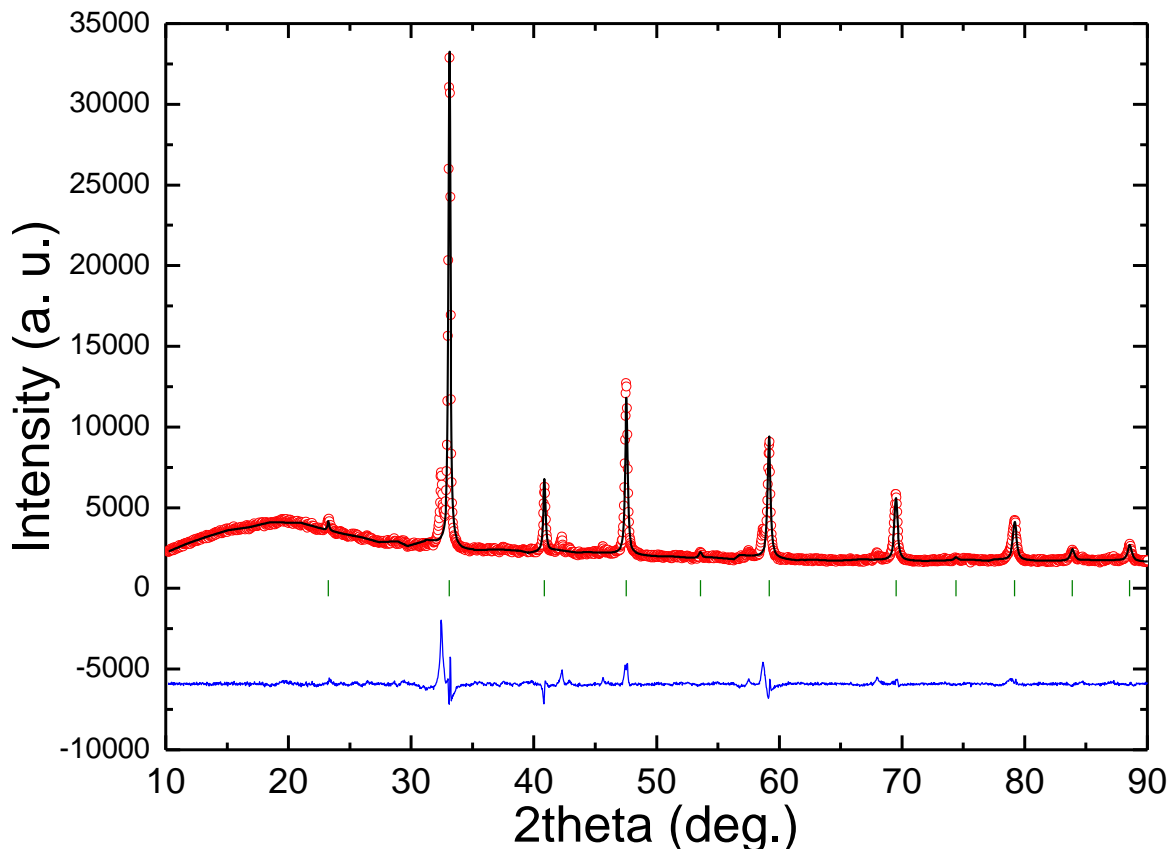


**Fig. 1.** Rietveld refinement of the powder XRD pattern taking into account only the  $\text{SrCrO}_3$  phase. The pattern exhibits the experimental (red circles), calculated (black line) and difference (blue line) curves in the range  $2\theta = 10.2^\circ - 90.3^\circ$  ( $R_{\text{Bragg}} = 5.17\%$  and global  $\chi^2 = 19.2\%$ ). Green vertical markers refer to the calculated positions of the Bragg reflections for  $\text{SrCrO}_3$ .

### 3.1 Imaging, EDS analysis and SAED

TEM imaging and EDS analysis were carried out on over 40 particles, exhibiting three types of particles, easily recognizable thanks to their shape and their cationic ratio. In figure 2 (a) the rods surrounded by red hatched circles correspond to crystallized particles with the cationic ratio:  $\text{Sr}/\text{Cr} \approx 57\%/43\%$  (the Sr4310 phase), the bigger crystallized particles correspond to the cationic ratio  $\text{Sr}/\text{Cr} \approx 50\%/50\%$  (majority perovskite  $\text{SrCrO}_3$  phase) and the “stringy-shaped”

particles (100 % Sr from EDS and amorphous phase according to SAED carried out on it) are very likely hydrated SrO precursor  $\text{Sr}(\text{OH})_2(\text{H}_2\text{O})_x$ .

Several ED patterns of the Sr4310 were recorded in zone axis by tilting around crystallographic axes for the unit cell and extinction conditions determination. The reconstruction of the reciprocal space confirmed the tetragonal unit cell with the parameters  $a \approx 3.9 \text{ \AA}$  and  $c \approx 28 \text{ \AA}$  (Fig. 2 (b)) previously determined by XRD. The extinction conditions on hkl reflections are consistent with a body-centered I lattice type and no other extra conditions were observed.

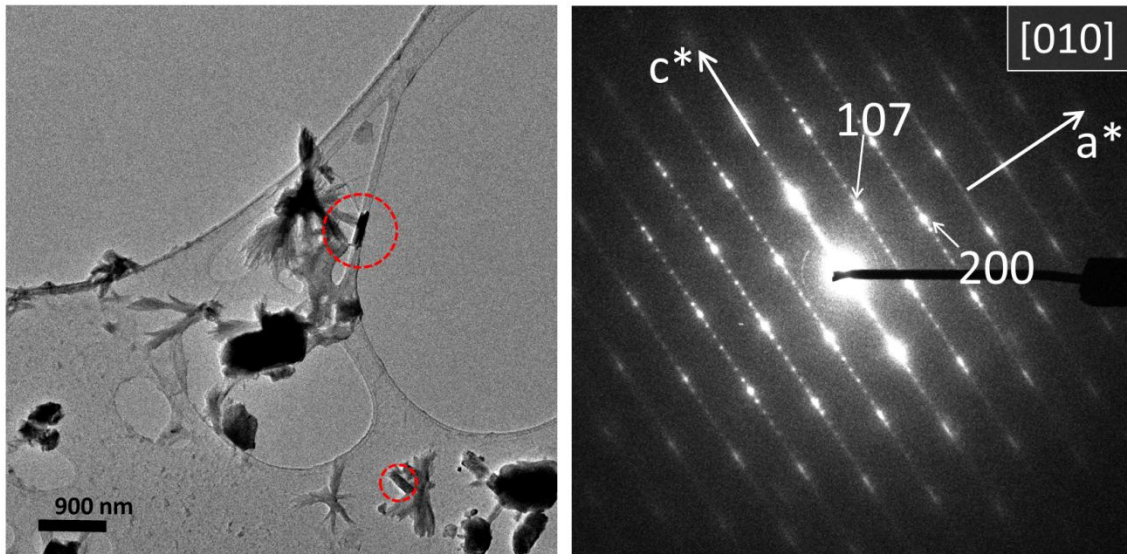


**Fig. 2.** (a) Low resolution TEM image of the particles contained in the powder. The small needle-shaped particles highlighted by red dashed circles correspond to the  $\text{Sr}_4\text{Cr}_3\text{O}_{10}$  phase. (b) [010] Zone axis SAED pattern of a  $\text{Sr}_4\text{Cr}_3\text{O}_{10}$  particle.

### 3.2. Precession Electron Diffraction :

Extraction of reflection intensities of each PED pattern was performed by integrating the intensity of each reflection after subtracting the background noise. Consequently 5 different datasets were created from the zone axes PED patterns [010], [1-40], [1-30], [1-20], [2-30] (Fig. 3) and merged using the common reflections between patterns. This process gave rise to reliability factor  $R_{\text{merge}}$  lower than 8%, confirming the good homogeneity between intensities of the common reflections. A second merge step was carried out by applying the most symmetrical space group  $I4/mmm$ , giving rise to 556 independent reflections with a satisfactory  $R_{\text{sym}}$  of 2.7%.

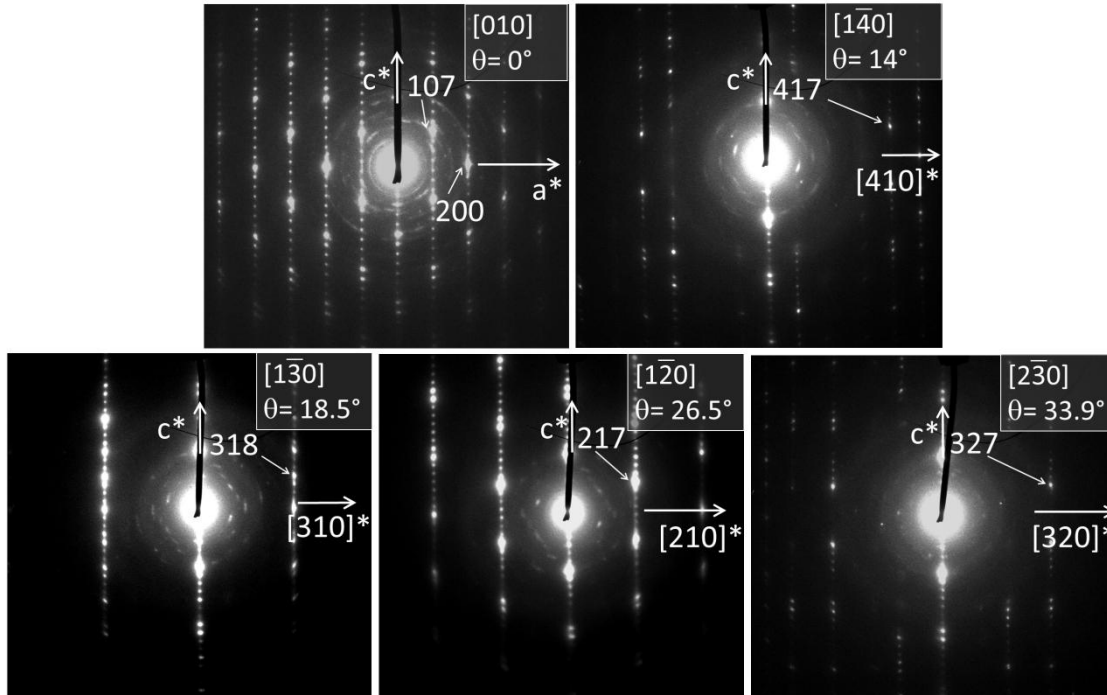


**Fig. 3.** Zone axis PED patterns recorded by turning around  $c$  axis of  $\text{Sr}_4\text{Cr}_3\text{O}_{10}$ .

Combining the EDS cationic ratio  $\text{Sr}/\text{Cr} = 57\%/43\%$  with the attribution of  $2+$  valency for strontium and  $4+$  for chromium, the chemical formula  $\text{Sr}_{1.14}\text{Cr}_{0.86}\text{O}_{2.86}$  was deduced. To calculate the number of atoms per unit cell, the number of atoms in the cubic perovskite  $\text{SrCrO}_3$  was then considered. The  $c$ -axis parameter is almost 7 times larger than the perovskite lattice parameter, which leads to this chemical composition of the unit cell :  $7 \times \text{Sr}_{1.14}\text{Cr}_{0.86}\text{O}_{2.86} \approx \text{Sr}_8\text{Cr}_6\text{O}_{20}$ .

A structural model was calculated by SIR 2011 in the  $I 4/mmm$  space group using the two-beam approximation of dynamical theory  $I_{\text{hkl}} \propto |F_{\text{hkl}}|$  which assumes that only the incident and the diffracted beams interact in the crystal. Varying the resolution values between  $0.8 \text{ \AA}$  and  $1.0 \text{ \AA}$  gave realistic solutions in term of cationic positions. Fig. 4 (a) exhibits the Fourier maps for  $y = 0$  and  $y = 0.5$  of the solution for a resolution value of  $1.0 \text{ \AA}$  : **for such a resolution value, 74 independent reflections were taken into account, leading to a satisfactory completeness of 74%, the other 482 reflections were rejected by SIR2011 since they were over  $1.0 \text{ \AA}$ .** The corresponding structural model is depicted in Fig. 4 (b). The structure consists of a regular stacking along  $c$ -axis of  $\text{SrO}_x$  sheets with  $\text{CrO}_x$  sheets, the Cr-Cr and Sr-Sr distances are all approximately equal to  $3.9 \text{ \AA}$  along  $a$ - and  $b$ -axes. However the number of oxygen atoms of the model is too high and not realistic for such a unit cell (56 instead of 20 expected) and several O-O distances are too short ( $\text{O1-O1} = 1.3 \text{ \AA}$ ,  $\text{O2-O2} = 1.5 \text{ \AA}$ ,  $\text{O3-O3} = 1.1 \text{ \AA}$  and  $\text{O4-O4} = 0.9 \text{ \AA}$ ), **forming oxygen clusters as highlighted by dashed circles in Fig. 4(b).** In order to reduce the oxygen number with O-O distances physically acceptable, oxygen atoms were placed in special positions as followed :

- O1 16n ( $1/2, 0.83, 0.15$ ) becomes O1 8g ( $1/2, 0, 0.15$ )

- O2 16n (1/2, 0.40, 0.07) becomes O2 4e (1/2, 1/2, 0.07)
- O3 8i (1/2, 0.88, 0) becomes O3 4c (1/2, 0, 0)
- O4 16n (1/2, 0.41, 0.2) becomes O4 4e (1/2, 1/2, 0.2)

Lastly, the unit cell contains 20 oxygens, which is consistent with the oxygen number calculated considering the valency states of Cr and Sr. All chromium cations are surrounded by 6 oxygens in octahedral environment, with Cr-O bond lengths between 1.8 Å and 2.1 Å, in agreement with the calculated distance from the respective theoretical ionic radius of Cr<sup>4+</sup> (0.55 Å) and O<sup>2-</sup> (1.40 Å) [13].

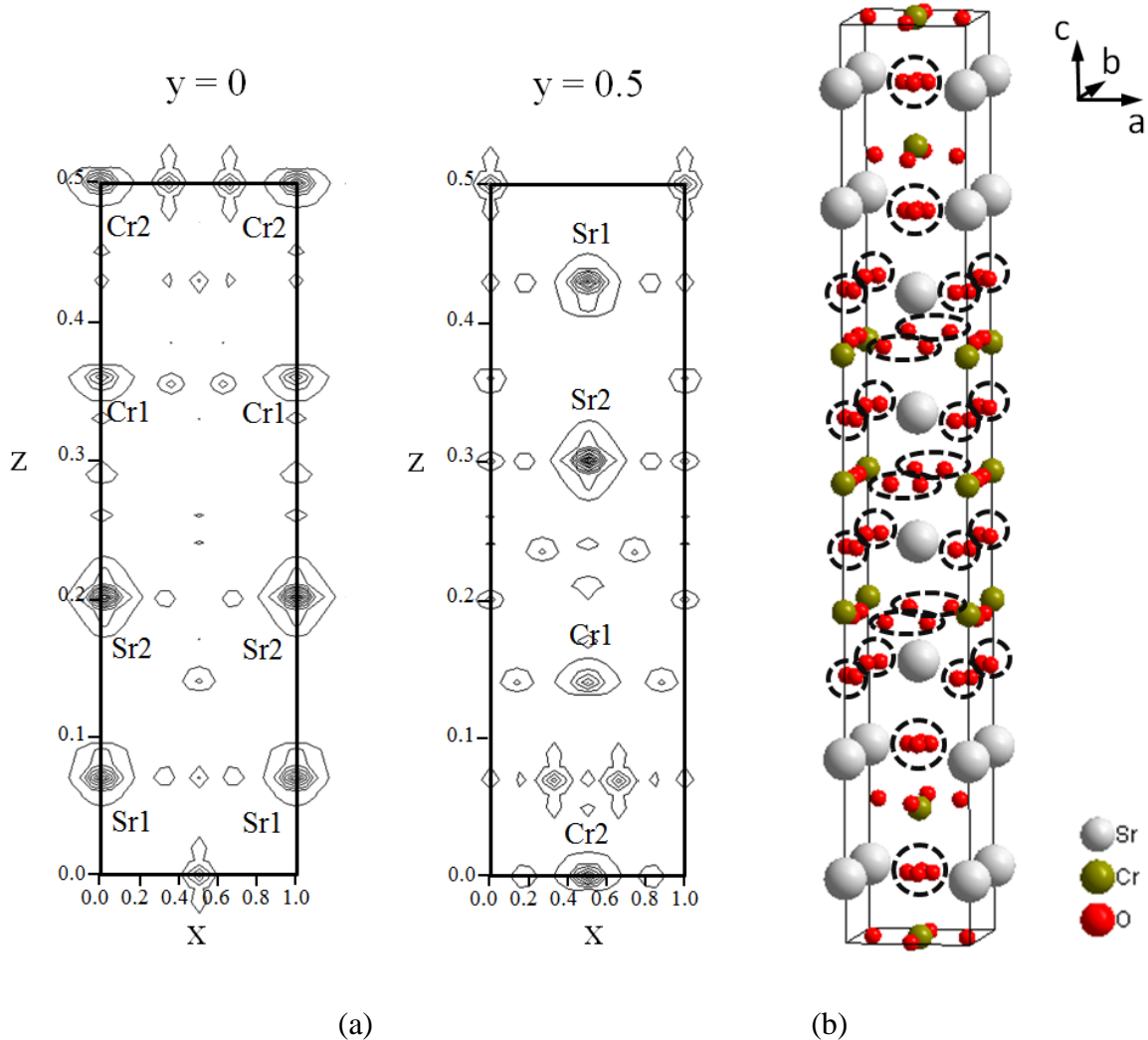


**Fig. 4.** (a) Fourier maps calculated for  $d_{\text{resolution}} = 1.0 \text{ \AA}$  at  $y = 0$  and  $y = 0.5$ . The electrostatic potentials emphasize the cationic sites, (b) Corresponding raw structural model calculated by SIR2011.

### 3.3. Final structural model of Sr<sub>4</sub>Cr<sub>3</sub>O<sub>10</sub> from XRD refinement

The structural model of Sr<sub>4</sub>Cr<sub>3</sub>O<sub>10</sub> established by electron diffraction was refined using the Rietveld method applied on the powder XRD pattern. Only the main Sr<sub>4</sub>Cr<sub>3</sub>O<sub>10</sub> and SrCrO<sub>3</sub>

phases were taken into account, the minority (hydrated and non magnetic) Sr oxide phase giving no detectable Bragg peaks in the XRD experiment. The parameters of profile function of the diffraction peaks were evaluated by the Caglioti equation [14]. The cell parameters of both  $\text{Sr}_4\text{Cr}_3\text{O}_{10}$  and  $\text{SrCrO}_3$  phases were first refined using the Le Bail method. Then, the atomic positions and scaling factors of both phases were refined using the Rietveld method. The isotropic thermal factors were maintained fixed ( $B_{\text{iso}} = 0.5 \text{ \AA}^2$  for Sr and Cr, and  $B_{\text{iso}} = 1 \text{ \AA}^2$  for O) **and some Cr-O distances were restrained to 2 \AA in order to avoid a too large variation of the oxygen positions during the refinement.** The refinement led to satisfactory reliability factors  $R_{\text{Bragg}}$  and  $\chi^2$ , and a good match between experimental and calculated XRD diagrams. Details of the refinement conditions, cell parameters and reliability factors are given in Table 1. Atomic positions and interatomic bond distances are given respectively in Tables 2 and 3.

The observed and calculated XRD diagrams with their difference curve are presented in Fig. 5, showing a good agreement between observed and calculated diffraction profiles. Finally, from the refinement the relative ratio between  $\text{Sr}_4\text{Cr}_3\text{O}_{10}$  and  $\text{SrCrO}_3$  was found to be 22.9 % (0.1) and 77.1 % (0.1), respectively. The refined crystallographic structure  $\text{Sr}_4\text{Cr}_3\text{O}_{10}$  is depicted in Fig. 5. It consists of triple perovskite  $[\text{SrCrO}_3]_3$  layers stacking separated by a single rock-salt layer  $[\text{SrO}]$ , as expected for the  $n = 3$  member of the Ruddlesden-Popper family with general formula  $[\text{ABO}]_n[\text{AO}]$ . Because x-ray diffraction is not well adapted to determine position of light atoms like oxygen (in the presence of heavier atoms like Cr and Sr in the lattice) neutron powder diffraction on  $\text{Sr}_4\text{Cr}_3\text{O}_{10}$  would be of great interest **to get reliable O1, O2 and O4 oxygen positions and discuss the potential distortions of  $\text{CrO}_6$  octahedron around each Cr1 and Cr2 sites.**

| Results obtained from Rietveld's profile analysis method                                  |             |
|---|-------------|
| Step scan increment ( $^{\circ}2\theta$ )   | 0.03        |
| $2\theta$ range ( $^{\circ}$ )  | 10.2 -90.3  |
| <b>phase 1 : SrCrO<sub>3</sub> (space group P m<math>\bar{3}</math>m / Z = 1)</b>         |             |
| scale factor  | 0.0304(2)   |
| U   | 0.05(2)     |
| V   | 0.08(2)     |
| W   | 0.009(4)    |
| shape   | 0.61(2)     |
| a( $\text{\AA}$ )   | 3.82126(9)  |
| V( $\text{\AA}^3$ )   | 55.798(2)   |
| R <sub>Bragg</sub> (%)  | 1.75        |
| <b>phase 2 : Sr<sub>4</sub>Cr<sub>3</sub>O<sub>10</sub> (space group I 4/mmm / Z = 2)</b> |             |
| scale factor  | 0.000162(3) |
| U   | 0.1(1)      |
| V   | 0.03(9)     |
| W   | 0.06(2)     |
| shape   | 0.86(4)     |
| a( $\text{\AA}$ )   | 3.8278(2)   |
| c( $\text{\AA}$ )   | 27.795(3)   |
| V( $\text{\AA}^3$ )   | 407.24(5)   |
| R <sub>Bragg</sub> (%)  | 5.95        |
| global $\chi^2$ (%)   | 1.98        |

**Table 1 : Parameters and reliability factors after the Rietveld refinement of the X-ray diffraction pattern with both phases SrCrO<sub>3</sub> and Sr<sub>4</sub>Cr<sub>3</sub>O<sub>10</sub>.**

|     | Site | x   | y   | z         |
|-----|------|-----|-----|-----------|
| Sr1 | 4e   | 0   | 0   | 0.0704(7) |
| Sr2 | 4e   | 0   | 0   | 0.2041(5) |
| Cr1 | 4e   | 0.5 | 0.5 | 0.139(1)  |
| Cr2 | 2b   | 0.5 | 0.5 | 0         |
| O1  | 8g   | 0.5 | 0   | 0.136(2)  |
| O2  | 4e   | 0.5 | 0.5 | 0.068(4)  |
| O3  | 4c   | 0.5 | 0   | 0         |
| O4  | 4e   | 0.5 | 0.5 | 0.202(3)  |

**Table 2 : Atomic positions in Sr<sub>4</sub>Cr<sub>3</sub>O<sub>10</sub> after Rietveld refinement.**

| Atom1 | Atom2  | d(Å)      |
|-------|--------|-----------|
| Sr1   | O1(x4) | 2.64(4)   |
| Sr1   | O2(x4) | 2.707(3)  |
| Sr1   | O3(x4) | 2.74(1)   |
| Sr2   | O1(x4) | 2.69(4)   |
| Sr2   | O4(x4) | 2.707(2)  |
| Sr2   | O4     | 2.61(8)   |
| Cr1   | O1(x4) | 1.915(3)  |
| Cr1   | O2     | 1.9(1)    |
| Cr1   | O4     | 1.76(9)   |
| Cr2   | O2(x2) | 1.9(1)    |
| Cr2   | O3(x4) | 1.9139(1) |

**Table 3 : Selected interatomic distances (Å) for Sr<sub>4</sub>Cr<sub>3</sub>O<sub>10</sub>.**

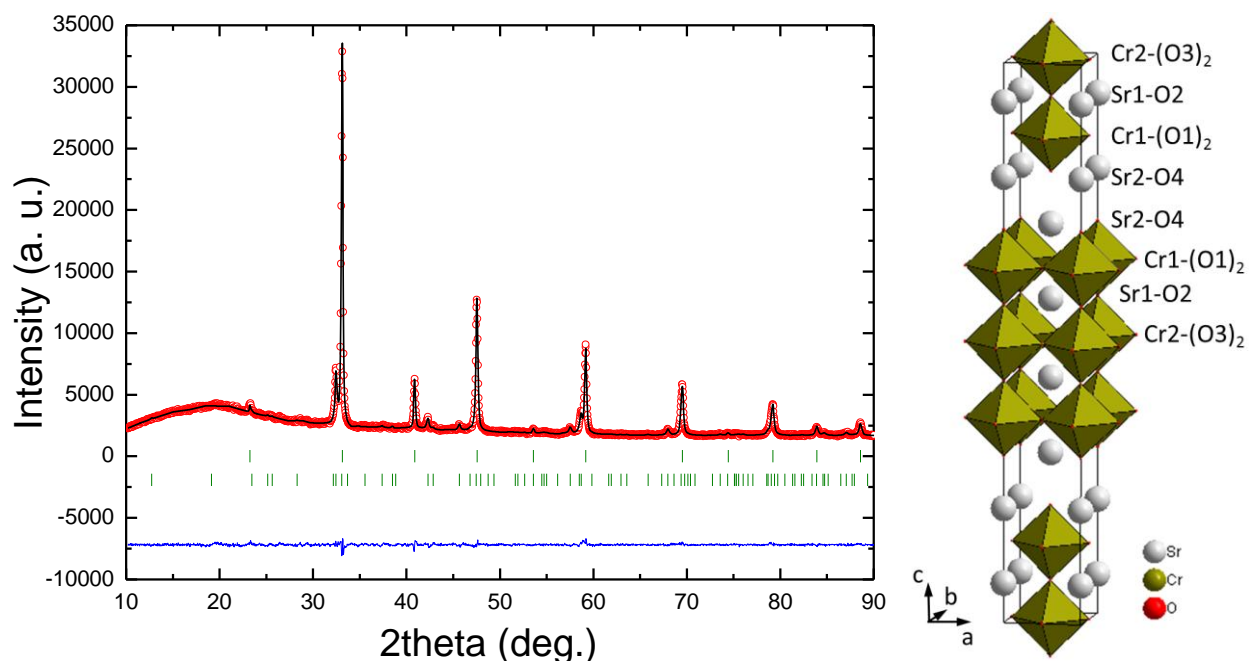


**Fig. 5.** Left: final Rietveld refinement. The pattern exhibits the experimental (red circles), calculated (black line) and difference (blue line) curves in the range  $2\theta = 10.2^\circ - 90.3^\circ$ . The last two lines with green vertical markers refer respectively to the calculated positions of the Bragg reflections for SrCrO<sub>3</sub> and Sr<sub>4</sub>Cr<sub>3</sub>O<sub>10</sub>. Right: schematical representation of the refined structure of Sr<sub>4</sub>Cr<sub>3</sub>O<sub>10</sub> with chemical composition of the different layers (see Table 2 for labels of atoms).

### 3.4 Physical properties

We present on Fig. 6 the electrical resistivities normalized at 300 K of the sample containing ~23% of  $\text{Sr}_4\text{Cr}_3\text{O}_{10}$  phase. We compare it to the typical curve obtained for a pure perovskite  $\text{SrCrO}_3$  sample (not discussed in this paper, see also published data in ref.16,17,20) synthesized in similar P,T conditions (but starting from a 1:1 molar ratio for  $\text{SrO}:\text{CrO}_2$ ).

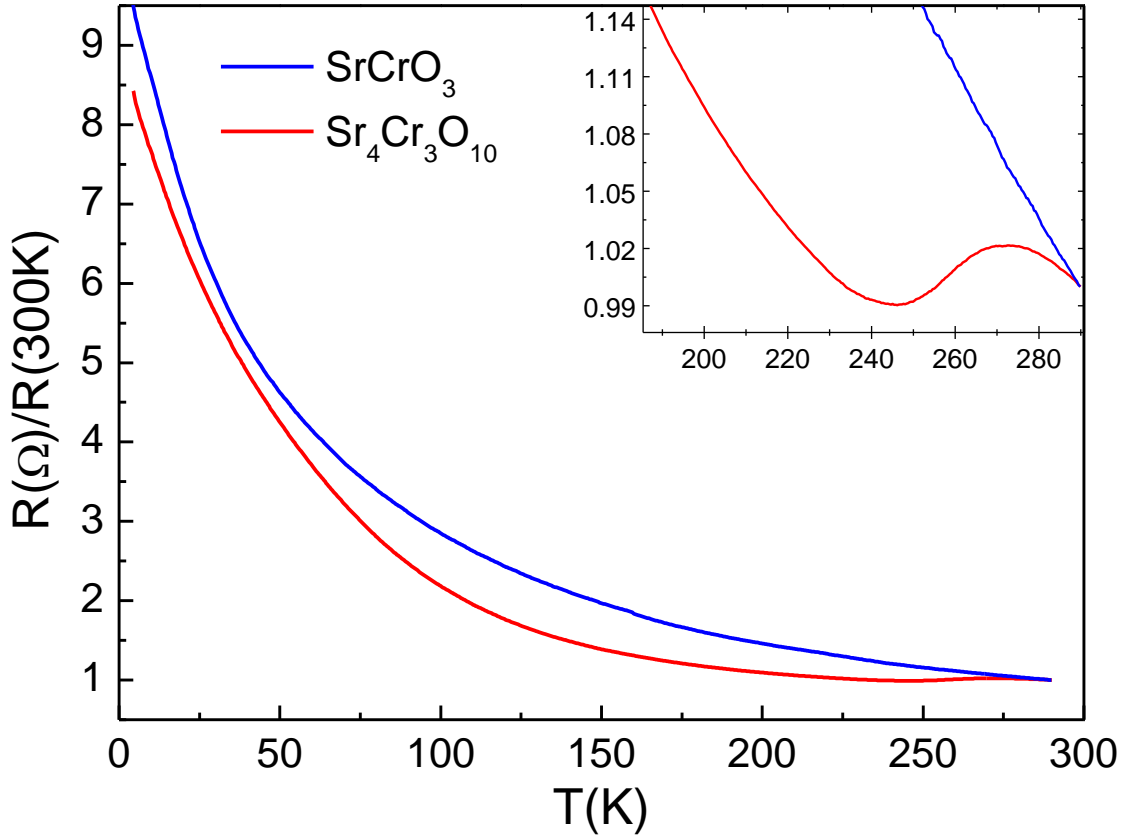


**Fig. 6.** Temperature dependence of the electrical resistivity of a polycrystalline  $\text{Sr}_4\text{Cr}_3\text{O}_{10}$  sample (in red) compared to the one of  $\text{SrCrO}_3$  (in blue) normalized to its room temperature value.

Both samples exhibit an insulating behavior but an anomaly is seen between 250 and 300 K (see inset) in the sample containing the  $n=3$  member of series. Thus, this anomaly corresponding to a crossover between two insulating state is intrinsic of the  $\text{Sr}_4\text{Cr}_3\text{O}_{10}$  phase.

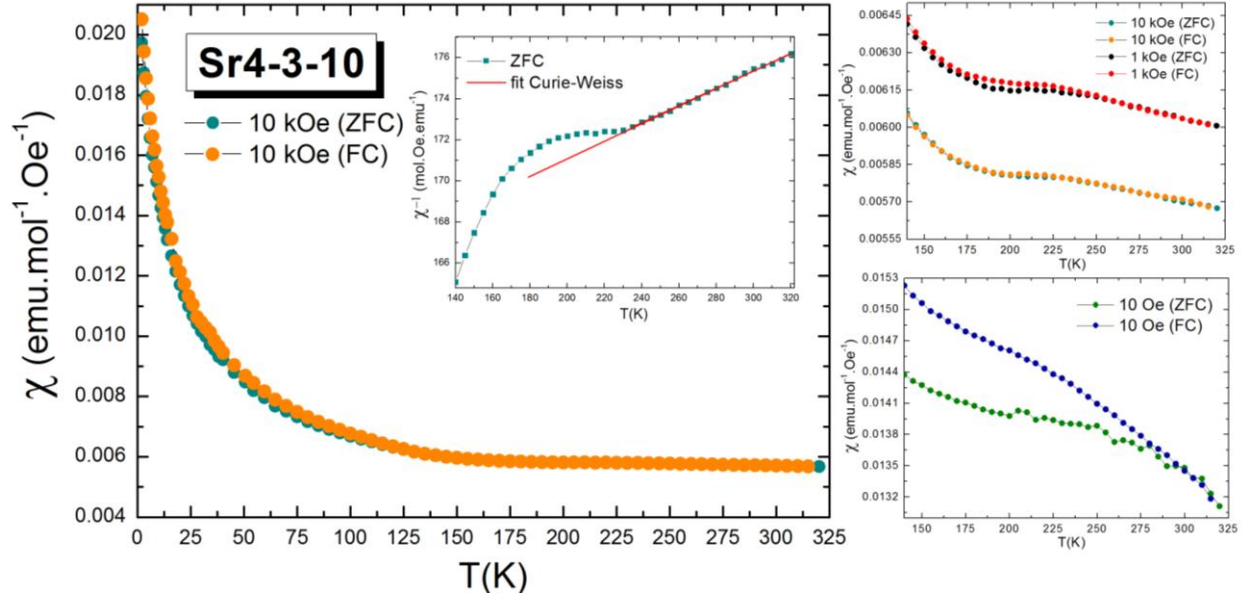


**Fig. 7.** Left panel : temperature dependence of the magnetic susceptibility of  $\text{Sr}_4\text{Cr}_3\text{O}_{10}$  measured at  $H = 1\text{ T}$  (10 kOe) in ZFC and FC conditions; inset of left panel: temperature dependence of the inverse of magnetic susceptibility. Right panel: enlarged view around 250-280K of the magnetic susceptibility at 0.1T (1kOe) and 1T (top figure) and at  $H=0.001\text{ T}$  (10Oe) (bottom figure).

Magnetization measurements performed between 2 and 320 K (Fig. 7) confirm this anomaly. It is very clear at low field, with the appearance of a kink around 280 K in the zero field cooled (ZFC) curve and a very distinct hysteresis between the ZFC and FC curves below 280 K. Both the characteristic temperature associated with the slope change and the amplitude of the magnetization hysteresis decrease with an increase of the magnetic field. Such magnetic behavior was never observed either in our pure  $\text{SrCrO}_3$  samples or in the literature [15,16,17]; in some  $\text{SrCrO}_3$  samples an anomaly is sometimes observed around 40K, not at 280 K, which is associated with a partial transition of the sample towards an AFM tetragonal phase, depending on the strain state of the sample (related to its pressure synthesis) [18,19,20]. Then, we attribute the kink at 280 K to an AFM transition of the  $\text{Sr}_4\text{Cr}_3\text{O}_{10}$  chromate. This signature of the AFM transition in Sr4310 is observed on a large paramagnetic background. At 1 T, the inverse susceptibility presented in the insert of left panel in Fig. 7 shows that the magnetization perfectly obeys a Curie-Weiss law above 240 K, with a Curie temperature  $\theta = -3867\text{ K}$ . This strong negative value of  $\theta$  is difficult to interpret because our magnetization measurement corresponds to the mixed behavior of both Sr4310 and perovskite phases. For the same reason, it is also not possible to correctly estimate the effective magnetic moment of  $\text{Cr}^{4+}$  in Sr4310. To go deeper in the determination of the electronic properties of  $\text{Sr}_4\text{Cr}_3\text{O}_{10}$  a monophasic sample is necessary.

## Conclusion

The  $n=3$  member of the  $\text{Sr}_{n+1}\text{Cr}_n\text{O}_{3n+1}$ , namely  $\text{Sr}_4\text{Cr}_3\text{O}_{10}$ , a high pressure phase, was clearly identified in a sample containing in majority the perovskite  $\text{SrCrO}_3$ . Thanks to a combined use of x-ray and electron diffractions, we have resolved for the first time its crystallographic

structure. Moreover, as for the other members of the  $\text{Sr}_{n+1}\text{Cr}_n\text{O}_{3n+1}$  series, in their polycrystalline form, we show that  $\text{Sr}_4\text{Cr}_3\text{O}_{10}$  (Sr4310) is an insulating chromate with an antiferromagnetic (AFM) transition at  $T_N=280\text{K}$ .

## Acknowledgments

The authors acknowledge C. Goujon and M. Legendre for their help in the use of the Conac large volume press during the HP-HT synthesis of our samples. We also thank U. Haselmann who was involved in the TEM study of our sample during his Master 1 internship at Néel Institute and H. Klein for a valuable reading of our manuscript. J. Jeanneau thanks the French state funds ANR-10-LABX-51-01 for the financial support of his PhD salary.

## References

- 
- [1] J.G. Bednorz and K.A. Müller, *Z. Phys. B - Condensed Matter* 64 (1986) 189-193.
  - [2] M. Imada, Fujimori, A. Fujimori, Y. Tokura, *Reviews of Modern Physics* 70 (1998) 1039.
  - [3] E. Dagotto, T. Hottab, A. Moreo, *Physics Reports* 344 (2001) 1.
  - [4] J. A. Kafalas and J. M. Longo, *J. Sol. St. Chem.* 4 (1972) 55-59.
  - [5] J. Jeanneau, P. Toulemonde, Manuel Nunez-Regueiro *et al.*, submitted to *Phys. Rev. Lett.* (2016).
  - [6] E. Castillo-Martinez, M.A. Alario-Franco, *Solid State Sciences* 9 (2007) 564.
  - [7] L. G. Khvostantsev, V. N. Slesarev, and V. V. Brazhkin, *High Pressure Research* 24 (2004) 371.
  - [8] C. Goujon, M. Legendre, P. Plaindoux, A. Prat and R. Bruyère, *High Pressure Research* 31 (2011) 375.
  - [9] X. Zou, Y. Sukharev, S. Hovmöller, *Ultramicroscopy* 49 (1993) 147.
  - [10] G.L. Cascarano, C. Giacovazzo, B. Carrozzini, *Ultramicroscopy* 111 (2010) 56.
  - [11] S.N. Ruddlesden and P. Popper, *Acta Cryst.* 10 (1957) 538.
  - [12] S.N. Ruddlesden and P. Popper, *Acta Cryst.* 11 (1958) 54.
  - [13] R.D. Shannon, *Acta Cryst.* A32 (1976) 751.
  - [14] G. Caglioti, A. Paoletti, F.P. Ricci, *Nucl. Instrum.* 3 (1958) 223.
  - [15] B. L. Chamberland, *Solid State Comm.* 5 (1967) 663.
  - [16] J.-S. Zhou, C.-Q. Jin, Y.-W. Long, L.-X. Yang, and J. B. Goodenough, *Phys. Rev. Lett.* 96 (2006) 046408.
  - [17] L.P. Cao *et al.* *Int. J. Mod. Phys B* 29 (2015) 1542025.
  - [18] A. J. Williams *et al.* *Phys. Rev. B* 73 (2006) 104409.
  - [19] L. Ortega-San-Martin, A. J. Williams, J. Rodgers, J. P. Attfield, G. Heymann, and H. Huppertz, *Phys. Rev. Lett.* 99 (2007) 255701.
  - [20] A.C. Komarek *et al.* *Phys. Rev. B* 84 (2011) 125114.